Permanent-Magnet-Free-Synchronous Motor with Self-Excited Wound-Field Technique Utilizing Space Harmonics

Masahiro Aoyama
Member, IEEE
SUZUKI Motor Corporation
300 Takatsuka-cho, Minami-ku, Hamamatsu
Shizuoka, Japan
aoyamam@hhq.suzuki.co.jp

Toshihiko Noguchi
Senior Member, IEEE
Shizuoka University
3-5-1, Johoku, Naka-ku, Hamamatsu
Shizuoka, Japan
noguchi.toshihiko@shizuoka.ac.jp

***Abstract* -- This paper describes a permanent-magnet-free synchronous motor where space harmonic power is utilized for the field magnetization instead of permanent magnets. The stator has a three-phase concentrated winding structure, and the rotor has two types of windings, i.e., an induction coil that retrieves mainly the second space harmonic and a field coil for the field magnetization. The two coils are connected via a center-tapped full bridge diode rectifying circuit. The principle of self-excitation utilizing space harmonics power is conducted, and the mathematical model is discussed. In addition, experimental test results are demonstrated compared with interior-permanent-magnet synchronous motor for HEV application.**

Keywords—*wound-field, synchronous motor, self-excitation, diode rectifier, space harmonics, induced current, concentrated winding stator, permanent-magnet-free, HEV application.*

I. INTRODUCTION

Recently, various technical portfolios for automotive application are considered, e.g., low-end hybrid system based on a 12-V idling stop system, and a high-efficiency power train technology with a high electrification ratio to achieve zero-emission [1],[2]. Regarding an electric-machine as an energy conversion device, an Interior Permanent Magnet Synchronous Motor (IPMSM) is commonly applied to Hybrid Vehicles (HEVs) and Electric Vehicles (EVs) because of its high efficiency [3][4]. Permanent magnets (PMs) used for the IPM motor are, however, very expensive because Nd-Fe-B magnets are generally employed to achieve higher energy density and to improve fuel efficiency at low-load operation for street used. Moreover, the traction motors are usually installed on the chassis, where special countermeasures must be taken from the viewpoints of environmental and thermal issues. In order to restrain demagnetization caused by the temperature rise of the PMs, for example, expensive rare-earth metals such as Dy and Tb must be added to Nd-Fe-B magnets. A material technology development, which is intensively placed Dy and Tb where the demagnetizing point easily, is actively engaged [5]. However, a global maldistribution problem of the natural resources such as Dy and Tb is not discussed. Therefore, varieties of PM-free motors, particularly wound-field (WF) synchronous motors which replaces PMs with electromagnet coils (E-coils) are focused on due to the recent market price spikes of Nd-Fe-B magnet [6]-[8]. These separated-excited WF machines, i.e., the WF flux switching motor have advantage in terms of a robust rotor structure for high-speed operation. The great merit of the high-speed operation is to reduce the weight of the machine. The torque density of these motors are, however, lower than that of IPMSM because it cannot utilize reluctance torque but only electromagnet torque which is generated by the DC field excitation.

Recently, the self-excited WF synchronous motor that can utilize the space harmonics for the field magnetization has been studied in the industries for the automotive traction application [9]-[11]. The classic self-excitation is roughly classified into three types. The former has additional auxiliary windings on the primary side for space harmonics generation utilizing self-excitation [12]-[14]. The second excites the armature windings with time harmonic injection, habitually [15],[16]. The third, however, can eliminate these auxiliary windings or time harmonic injection, because the space harmonics for the self-excitation can be obtained by the concentrated winding structure, automatically [9]-[11]. In addition, the third one has potential to obtain a position of the post IPMSM by achieving the comparable torque density with the PM-free configuration. Because it can utilize the reluctance torque and the self-excited electromagnet torque without any additional space harmonic excitation windings in the stator slots. In the past works, however, it cannot efficiently retrieve the space harmonics power [9]-[11]. The authors already proposed PM-free motor utilizing effectively the space harmonics for the field magnetization power [17]-[19]. In addition, the preliminary experimental test results for principle verification also reported in [20]. This proposed motor is the same self-excitation principle with the past

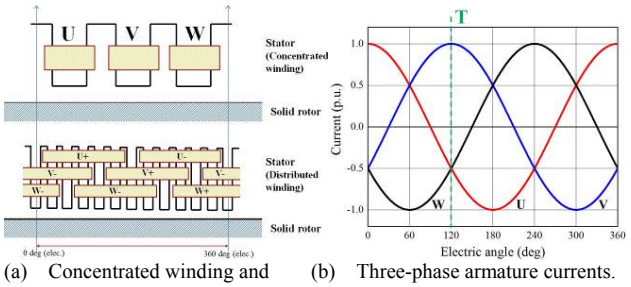

(a) Concentrated winding and distributed winding structure. (b) Three-phase armature currents.

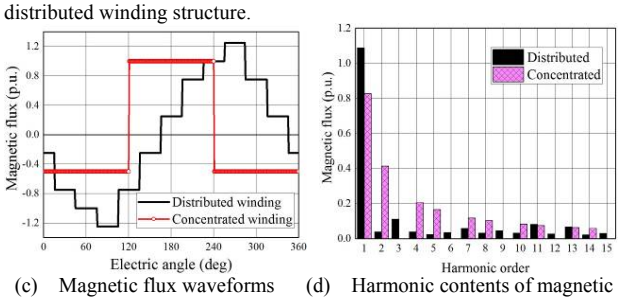

(c) Magnetic flux waveforms in air-gap at moment T in (b). (d) Harmonic contents of magnetic flux waveforms.

Fig. 1. Magnetic flux waveforms compared with concentrated winding and distributed winding structure and its harmonic contents.

works in [9],[10], but, it can efficiently retrieve the space harmonics by modifying rotor winding connection diagram, and placing auxiliary poles on the *q*-axis [17]. The proposed model in [17] can improve the stator-rotor coupling coefficient of the leakage magnetic flux by the effect of auxiliary poles compared with the benchmark model presented in [9]. The electromagnet torque caused by self-excitation and the reluctance torque caused by the saliency are simultaneously delivered in the proposed motor, but the electromagnet torque generated by the effect of auxiliary poles and the self-excited field current takes a significant part of the total torque. Because the reduction of the induced voltage in the rotor windings of the self-excited wound-field motor is hard to avoid in the low-speed range, the strong stator-rotor coupling coefficient of the leakage magnetic flux which generates the electromagnet torque is significantly important.

In this paper, a theoretical discussion of the proposed motor is conducted, and the mechanical designs are summarized. Then, the experimental test results focusing on the effects of auxiliary poles are demonstrated. In addition, the advantages are clarified by a comparison with benchmark IPMSM and prototype from the viewpoint of the adjustable speed drive characteristics and efficiency map.

II. Principle of Self-Excitation

A. Magnetomotive Force of Concentrated Winding Stator

The magnetomotive force generated by the concentrated winding structure contains the second-order space harmonic on the fundamental magnetic field. Figure 1 (a) shows a simplified stator winding structure of concentrated winding and distributed one, and Fig. 1 (c) shows the magnetic flux waveforms in air-gap at the moment T in Fig. 1 (b). Figure 1 (d) shows harmonic contents of the magnetic flux waveform in air-gap, which is analyzed by Fourier series and a developed formula of Fourier series of Fig. 1 (c). As can be seen in this Figure, the magnetic flux waveform of the distributed winding structure is basically sinusoidal, except for the slot harmonics. However, the waveform of the concentrated winding structure is distorted by the second-order harmonic component. The second-order harmonic component is caused because every phase winding is wound separately on an individual tooth without superposition on the other phase windings. In addition, this second space harmonic rotates in reverse direction of the fundamental rotating magnetic field direction.

Then, the relationship between a second space harmonic on static coordinates and a third time harmonic on the rotating reference frame are mathematically discussed. By approximating inductance with fundamental content and second-order content, the inductance in each phase (L_U, L_V, and L_W) on static coordinates can be given by

$$L_U(\theta) = -L_0 + L_{a1}\cos(\theta-\pi) + L_{a2}\cos(2\theta+\pi)\,, \quad (1)$$

$$L_V(\theta) = 2L_0 + L_{a1}\cos(\theta-\pi) + 2L_{a2}\cos(2\theta+\pi)\,, \text{ and} \quad (2)$$

$$L_W(\theta) = -L_0 + L_{a1}\cos(\theta-\pi) + L_{a2}\cos(2\theta+\pi)\,, \quad (3)$$

where L_0 is the constant part, and L_{a1} and L_{a2} are the amplitudes of the periodical variations. θ is a spatial rotor position. As can be seen in Eq. (1)-(3), it is confirmed that the second space harmonic rotates in reverse direction against the fundamental rotating magnetic field. By observing from rotor side, which means on the *dq*-reference frame, the second-order space harmonic can be observed as the third-time harmonic because of its reverse phase rotating direction, and it can be expressed as the following equation:

$$L_{sd}(t) = L_{sd0} + L_{sda}\cos 3\omega t\,, \text{ and} \quad (4),$$

$$L_{sq}(t) = L_{sq0} + L_{sqa}\cos(3\omega t - \pi/2)\,. \quad (5)$$

where L_{sd0}, and L_{sq0} is the constant part on *dq* reference frame. L_{sda}, and L_{sqa} is an amplitude of the harmonic inductance. The generalized voltage equation without mutual inductance can be given by

$$\begin{bmatrix} v_{sd} \\ v_{sq} \\ v_{rd} \\ v_{rq} \end{bmatrix} = \begin{bmatrix} R_s & 0 & 0 & 0 \\ 0 & R_s & 0 & 0 \\ 0 & 0 & R_s & 0 \\ 0 & 0 & 0 & R_s \end{bmatrix} \begin{bmatrix} i_{sd} \\ i_{sq} \\ i_{rd} \\ i_{rq} \end{bmatrix} + \begin{bmatrix} L_{sd0} & 0 & 0 & 0 \\ 0 & L_{sq0} & 0 & 0 \\ 0 & 0 & L_{rd0} & 0 \\ 0 & 0 & 0 & L_{rq0} \end{bmatrix} \begin{bmatrix} i_{sd} \\ i_{sq} \\ i_{rd} \\ i_{rq} \end{bmatrix} + \begin{bmatrix} \mathrm{p}L_{sd}(t) & -\omega L_{sq}(t) & \mathrm{p}M_{sdrd} & -\omega M_{sdrq} \\ \omega L_{sd}(t) & \mathrm{p}L_{sq}(t) & \omega M_{sqrd} & \mathrm{p}M_{sqrq} \\ \mathrm{p}M_{rdsd} & 0 & \mathrm{p}L_{rd}(t) & 0 \\ 0 & \mathrm{p}M_{rqsq} & 0 & \mathrm{p}L_{rq}(t) \end{bmatrix} \begin{bmatrix} i_{sd} \\ i_{sq} \\ i_{rd} \\ i_{rq} \end{bmatrix} \quad (6)$$

where v_{sd}, v_{sq}, i_{sd} and i_{sq} are the armature voltages and currents, v_{rd}, v_{rq}, i_{rd} and i_{rq} are the *d*-axis and *q*-axis rotor winding voltages, *M* means the mutual inductance between the stator and rotor, and currents, R_s and R_r are the armature winding and rotor winding resistances, and p denotes a differential operator, respectively. In the case of proposed

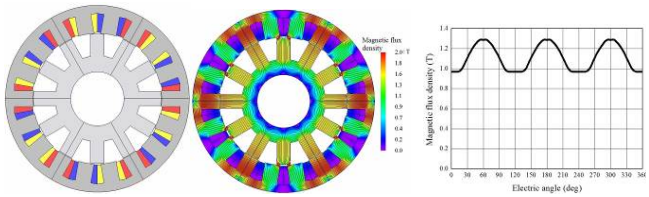

(a) 12poles-18slots motor. (b) *d*-axis inductance variation links around rotor salient pole surface.

Fig. 2. *d*-axis inductance variation of 12poles-18slots motor.

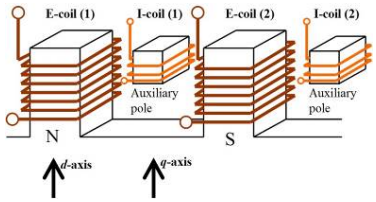

Fig. 3. Opened rotor winding diagram.

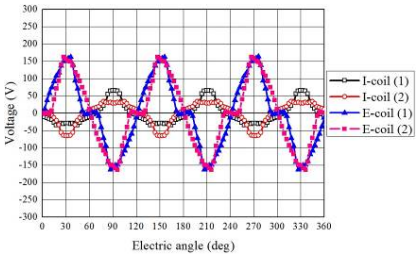

(a) Induced voltage on rotor windings.

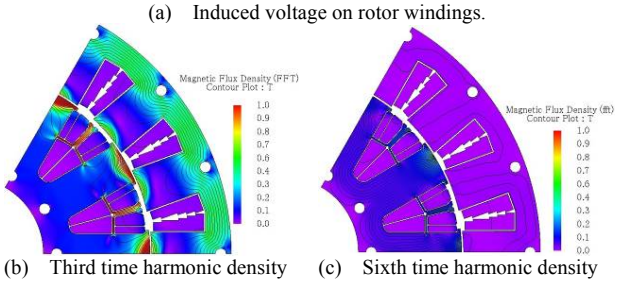

(b) Third time harmonic density and flux lines. (c) Sixth time harmonic density and flux lines.

Fig. 4. Simulation results under 1686 $A_{rms}T$, and current phase 0 deg for 1000 r/min.

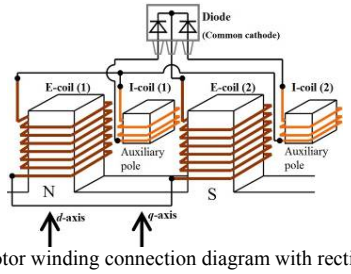

Fig. 5. Rotor winding connection diagram with rectifier circuit.

motor, the transformer EMF caused by the space harmonics, i.e., $pL_{sd}(t)$, and $pL_{sq}(t)$, makes the angular velocity EMF as shown in Eq. (7), and (8).

$$pL_{sd}(t) = \frac{d}{dt}\left\{L_{sd0} + L_{sda}\cos 3\omega t\right\} = -3\omega L_{sda}\sin 3\omega t \quad (7)$$

$$pL_{sq}(t) = -3\omega L_{sqa}\sin\left(3\omega t - \pi/2\right) \quad (8)$$

The induced voltage occurs by linking the asynchronous rotating magnetic field in Eq. (7), and (8) into rotor winding. After that, the field current can be obtained via a diode rectifier circuit on the rotor.

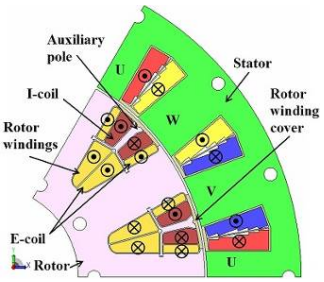

Fig. 6. Cross section (Circumferential direction: 1/6).

B. Slots Combination

Figure 2 shows magnetic flux density distributions of 12poles -18slots combination (2-to-3-slots-combination), and *d*-axis magnetic flux variation links around the rotor salient pole surface. As can be seen in the figure, the 2-to-3-slot-combination is the most efficient way to retrieve the third time harmonic power.

C. Self-Excitation Technique Utilizing Space Harmonics

The authors proposed the novel magnetic design that separates the induction coil (I-coil) from the electromagnet coil (E-coil) to improve the power retrieval efficiency [17]-[20]. From the authors' past investigation, the third time harmonic flux flows mainly through the rotor salient pole and the slot. Figure 3 shows a simplified rotor salient pole model and an auxiliary pole with opened rotor windings of the proposed motor. Figure 4 (a) shows the induced voltage waveforms of each coils in Fig. 3, i.e., an I-coil that retrieves mainly the *q*-axis third time harmonic, and an E-coil that retrieves the *d*-axis third time harmonic. This induced voltage is mainly caused by the linkage of the second space harmonic, which is automatically superimposed armature magnetomotive force of concentrated winding stator. Figure 4 (b), and (c) shows the third time harmonic and sixth time harmonic flux density contour and flux lines. It is found that the third time harmonic flux flows mainly through the rotor salient pole and the slot. This is the reason why the auxiliary pole should be placed on the *q*-axis, which is the most efficient way to retrieve the both of the *d*-axis and the *q*-axis space harmonic flux. Thus, the rotor windings should be better to connect via a center tapped diode rectifier as shown in Fig. 5. This rotor winding circuit can be reduced the number of diode module mounted on the rotor.

III. Configuration and Specifications of Proposed Motor

Figure 6 shows the cross section of proposed PM-free synchronous motor where the concentrated winding stator and the salient pole rotor with rectified rotor windings are employed. The rotor has two sorts of windings, as illustrated by a previous chapter. The I-coil is placed around the outer diameter part to retrieve the space harmonics power efficiently. In addition, the I-coil is magnetically independent

Table I. Specifications of prototype machine.

Number of poles	12
Number of slots	18
Stator outer diameter	200 mm
Rotor diameter	138.6 mm
Axial length of core	108 mm
Air gap length	0.7 mm
Maximum current	332.3 A_{rms} (60 s)
Stator winding resistance	10.5 mΩ / phase
Number of stator coil-turn	30 T/pole
Stator winding connection	6 parallel
Number of I-pole coil-turn	53
Number of E-pole coil turn	122
I-coil resistance	0.46 Ω / coil
E-coil resistance	1.18 Ω / coil
Thickness of iron core steel plate	0.30 mm (30DH)

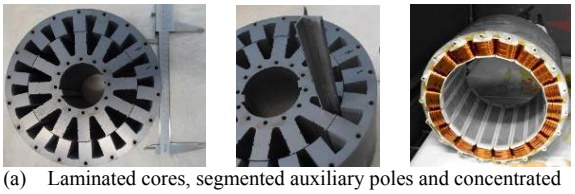

(a) Laminated cores, segmented auxiliary poles and concentrated winding stator.

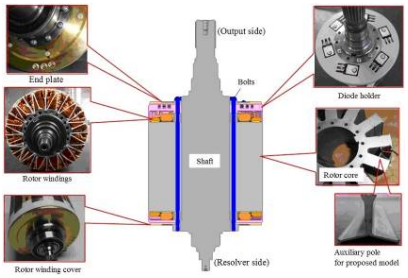

(b) Proposed self-excited wound-field rotor configuration.

Fig. 7. Prototype machine.

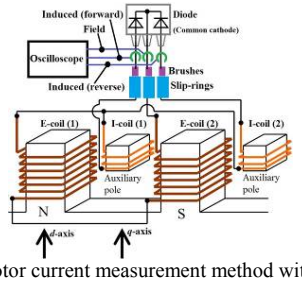

Fig. 8. Rotor current measurement method with slip-ring.

of the main magnetic flux path to prevent reduction of the saliency ratio. The I-poles, i.e., auxiliary poles, are fitted between the salient poles with wedge form and held from an axial direction using a rotor winding cover. On the other hand, each E-coil has saliency on the rotor for the field excitation, which uses the retrieved second space harmonic

(b) Benchmark model with slip-ring.

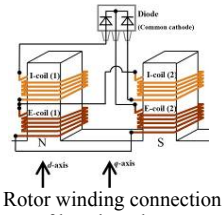

(c) Rotor winding connection diagram of benchmark.

Fig. 9. Benchmark model.

power. In addition, E-coil can retrieve the *d*-axis space harmonics. Specifications of the motor are listed in Table I.

IV. Prototype Machine

Figure 7 (a) shows motor cores of the actual prototype machine and the concentrated winding stator of prototype machine, which is applied rectangular wire for space factor improvement. The I-poles, i.e., auxiliary poles, are inserted in the rotor slots with wedge-formed beams, and are composed of iron core steel plate (30DH). Figure 7 (b) shows the proposed self-excited wound-field rotor of the prototype machine with a full-bridge rectifier mounted on the rotor windings. The wound-field rotor is mechanically reinforced by racing and a resin mold process to prevent destruction by the centrifugal force caused by a high speed rotation.

V. Experimental Test Results

A. *Effects of Auxiliary Poles*

The rotor induced current in the diode forward direction and the reverse direction for one pole pair is measured with a slip-ring to demonstrate the self-excitation by the third time harmonic as shown in Fig. 8. A benchmark model which has no-auxiliary poles in [10] is set up to clarify the advantages of proposed motor with auxiliary poles, experimentally. Figure 9 shows the benchmark model with a slip-ring, which is set up with the same rotor core of proposed motor without the auxiliary poles.

Figure 10 and Fig. 11 shows the stator armature current (U-phase) and rotor current waveforms (induced and field current) for 500 r/min under 414 A_{rms}T and 2000 r/min under 414 A_{rms}T of the stator armature magnetomotive force. The inverter carrier frequency is set at 10 kHz. In the experimental test, the load test of the motor is limited in the low-speed range. By referring to rotor current waveforms in Fig. 10 and Fig. 11, the induced current flows forward and reverse at time intervals. Thus, it can be easily confirmed that the third time harmonic on the rotating reference frame (the second space harmonic on static coordinates) links to rotor windings and the electromagnet poles can be obtained by field current generated with full-bridge rectifier as shown in Fig. 8. The adjustable speed drive characteristics with respect to current phase under armature magnetomotive force 210 A_{rms}T, 414 A_{rms}T, 620 A_{rms}T, and 825 A_{rms}T, which is shown in Fig. 13-16, of proposed and benchmark diode-rectifier PM-free motor as shown in Fig. 12, is investigated by

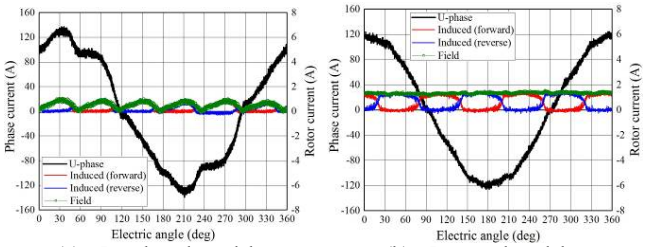

(a) Benchmark model. (b) Proposed model.

Fig. 10. Stator and rotor current waveforms under 414 $A_{rms}T$ and current phase 60 deg for 500 r/min.

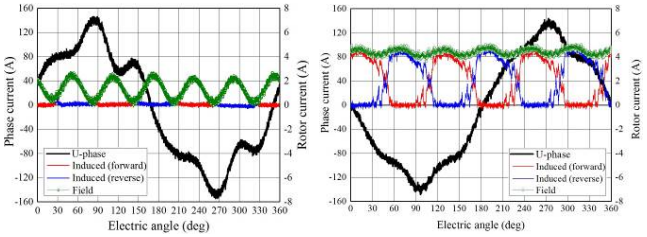

(a) Benchmark model. (b) Proposed model.

Fig. 11. Stator and rotor current waveforms under 414 $A_{rms}T$ and current phase 60 deg for 2000 r/min.

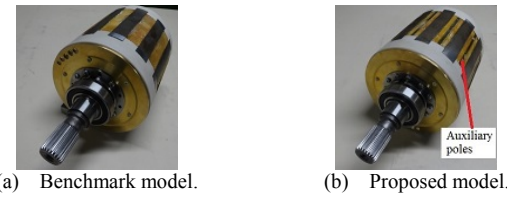

(a) Benchmark model. (b) Proposed model.

Fig. 12. Prototype rotor with diode rectifier circuit mounted on rotor windings.

controlling speed at a bench, and controlling torque with inverter. As shown in Fig. 13-16, it can be confirmed that the additional torque by the E-coils, i.e., self-excited electromagnet torque, greatly contributes to increase the total output torque with respect to rotation speed increase in addition to conventional torque, i.e., a reluctance torque. When the fundamental frequency is higher, the total torque shows a characteristic to increase because the time rate of change of the magnet flux linked to rotor winding is increase. Thus, the amplitude of the induced voltage base on Faraday's law, as a result, induced current increase, and electromagnet torque increase. Furthermore, the effects of torque performance improvement with modified rotor winding circuit and auxiliary poles of proposed motor can be confirmed as shown in Fig. 13-16. In details, the reluctance torque decreases with the effect of the saliency drop caused by the auxiliary poles, however, the electromagnet torque increases by improving the coupling coefficient between the stator and the rotor, i.e., mutual inductance, more than the decreases of reluctance torque. The increase of electromagnet torque means the rotor field magnetization increase as shown in Fig. 17, which is simulated by FE-analysis and visualized the magnetic flux density of the proposed motor.

Figure 18 and Fig. 19 presents the efficiency map in motoring and in regenerating compared with the benchmark model in Fig. 12 (a) and the proposed model in Fig. 12 (b).

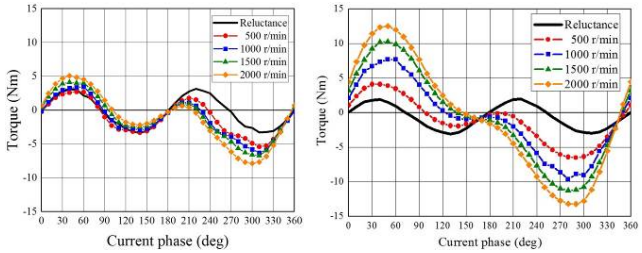

(a) Benchmark model. (b) Proposed model.

Fig. 13. Adjustable speed drive torque characteristics under 210 $A_{rms}T$.

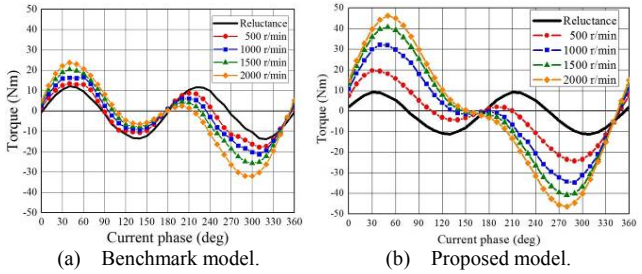

(a) Benchmark model. (b) Proposed model.

Fig. 14. Adjustable speed drive torque characteristics under 414 $A_{rms}T$.

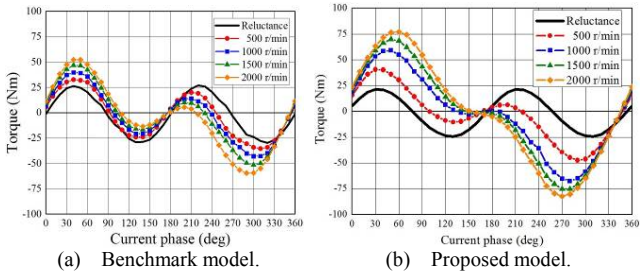

(a) Benchmark model. (b) Proposed model.

Fig. 15. Adjustable speed drive torque characteristics under 620 $A_{rms}T$.

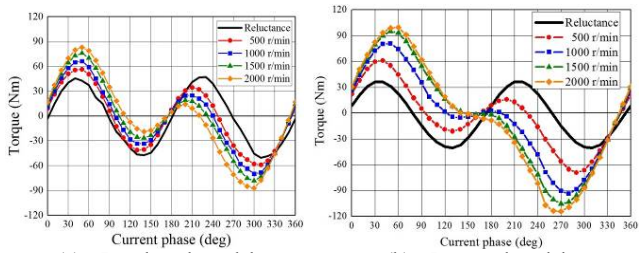

(a) Benchmark model. (b) Proposed model.

Fig. 16. Adjustable speed drive torque characteristics under 825 $A_{rms}T$.

The motor efficiency includes the rotor cupper loss caused by self-excitation utilizing space harmonics, iron loss, and the diode losses. Overall motor efficiency is quite good especially compared with classic permanent-magnet-free motors, e.g., an induction machine, a switched reluctance machine, and reluctance machine. Compared to the benchmark model, the proposed motor is performing better at all driving point, and can extremely improve the efficiency in low-speed area, especially. Figure 18 (c) shows the efficiency map with rotor winding opened in motoring, i.e., reluctance motor version of proposed motor. As can be confirmed in Fig. 18, self-excitation technique with auxiliary poles can extremely improve the motor efficiency. It is also confirmed that the auxiliary pole effects for efficiency improvement in regenerating as shown in Fig. 19.

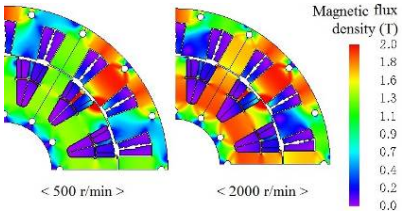

Fig. 17. Magnetic flux density simulated by FE-analysis.

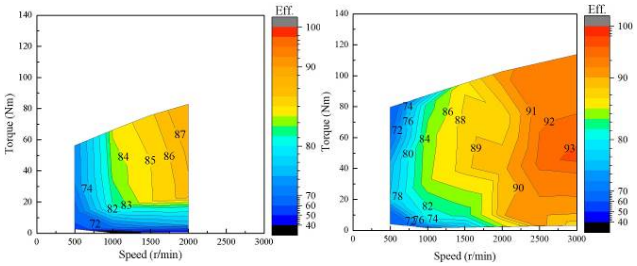

(a) Benchmark model. (b) Proposed model.

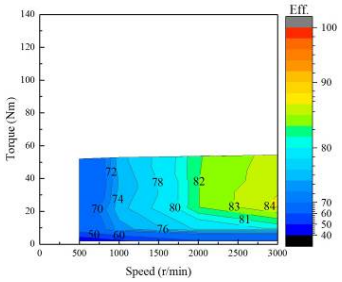

(c) Rotor winding opened of proposed model.

Fig. 18. Efficiency map in motoring.

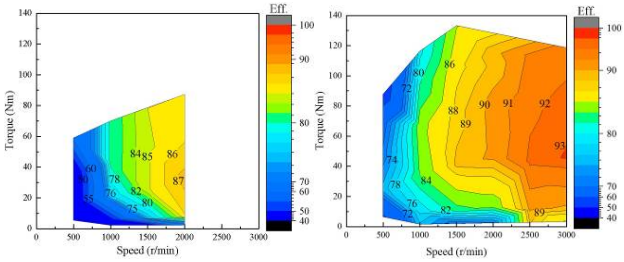

(a) Benchmark model. (b) Proposed model.

Fig. 19. Efficiency map in regenerating.

B. Compared with Benchmark IPMSM

Figure 20 shows the benchmark IPMSM with Nd-Fe-B magnets (B_r = 1.22 T, H_{cb} = 965.7 kA/m at 300 K), and distributed winding stator [21]. The laminated motor core size, (outer diameter, and stack length expect coil-end) of the benchmark IPMSM is the same as proposed motor listed in Tab. 1. Figure 21-23 shows the current phase vs. reluctance torque, magnet torque, and total torque characteristics, which is experimentally measured, of benchmark IPMSM and proposed motor, respectively. The proposed motor has a normal saliency; however, the benchmark IPMSM has an inverse saliency, so that the current phase-vs.-reluctance torque characteristics perform as shown in Fig. 21. It is exact that the benchmark IPMSM is generally more efficient than the proposed motor. However, the current phase-vs.-self-excited electromagnet torque characteristics are almost equal to benchmark IPMSM for 2000 r/min. As can be seen in Fig.

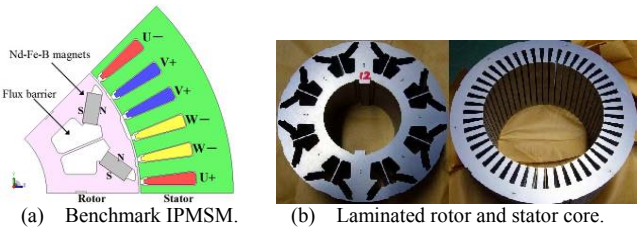

(a) Benchmark IPMSM. (b) Laminated rotor and stator core.

Fig. 20. Benchmark IPMSM with Nd-Fe-B magnets.

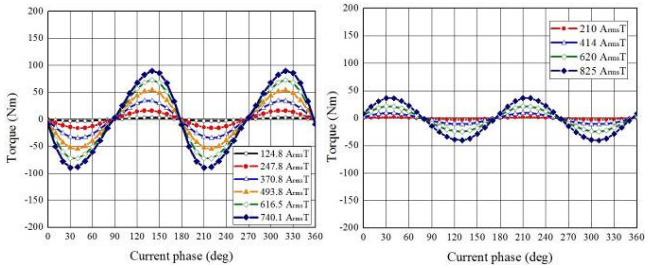

(a) Benchmark IPMSM. (b) Proposed motor.

Fig. 21. Current phase-vs.-reluctance torque characteristics.

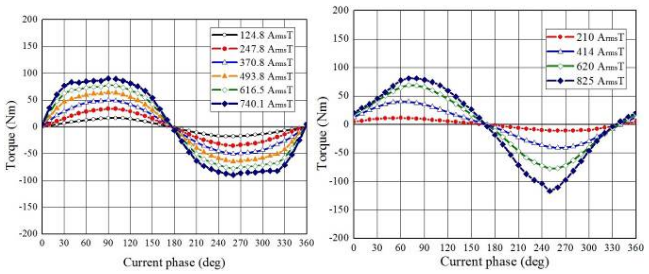

(a) Benchmark IPMSM. (b) Proposed motor.

Fig. 22. Current phase-vs.-magnet or self-excited electromagnet torque characteristics for 2000 r/min.

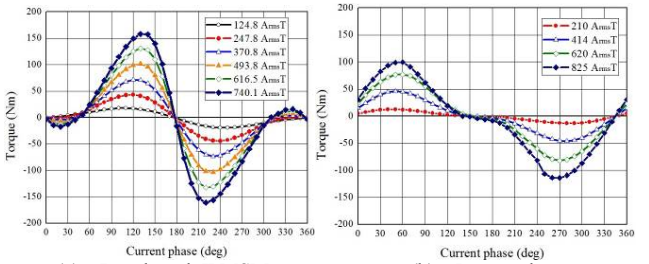

(a) Benchmark IPMSM. (b) Proposed motor.

Fig. 23. Current phase-vs.-total torque characteristics for 2000 r/min.

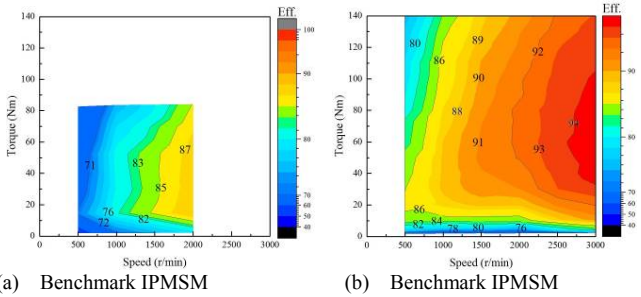

(a) Benchmark IPMSM without permanent-magnets. (b) Benchmark IPMSM with permanent-magnets.

Fig. 24. Efficiency map of benchmark IPMSM in motoring.

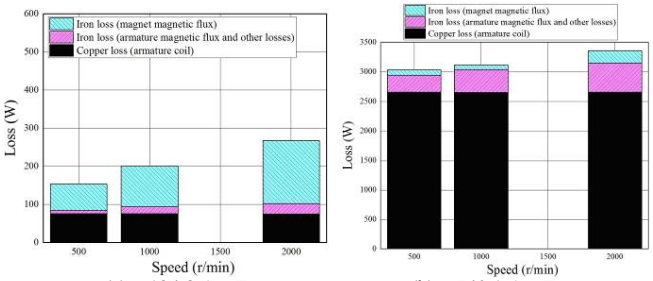

(a) 124.8 $A_{rms}T$. (b) 740.1 $A_{rms}T$.

Fig. 25. Measured loss details of benchmark IPMSM.

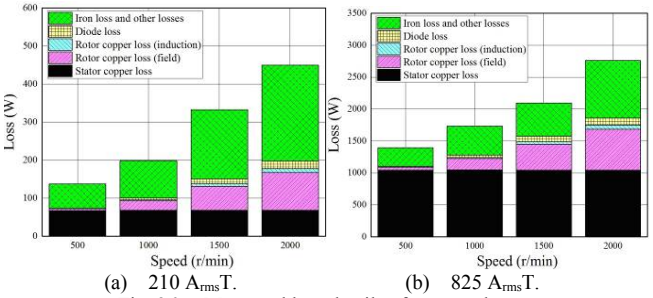

(a) 210 $A_{rms}T$. (b) 825 $A_{rms}T$.

Fig. 26. Measured loss details of proposed motor.

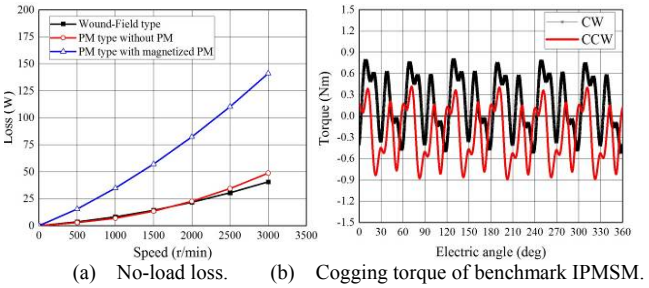

(a) No-load loss. (b) Cogging torque of benchmark IPMSM.

Fig. 27. Driving performance under no-load (measured).

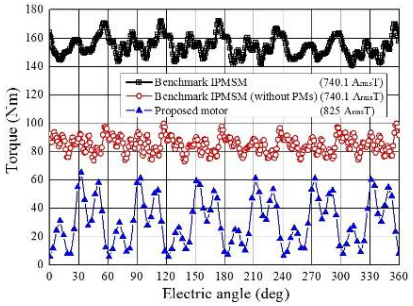

Fig. 28. Measured torque ripple for 100 r/min.

23, the total torque is lower than benchmark IPMSM below the middle armature magnetomotive force in spite of high electromagnet torque performance. It is because that the double saliency configuration has a large permeance variation, which causes the torque ripple increase, and magnetic flux is easy to be concentrated. This disadvantage causes the reluctance torque decreases by magnetic saturation. In addition, the low torque density in the extremely low-speed range is difficult to avoid because the amplitude of induced voltage in the rotor windings is based on Faraday's law. Around 0 r/min, torque density becomes low, although the high torque density is demanded for the automotive operation particular, e.g., bump ride-over. On the other hand, the passive magnetomotive force characteristic that is proportional to the armature current, current phase, and rotation speed is unique point as a variable magnetic flux motor. Figure 24 shows the efficiency map of benchmark IPMSM in motoring. As shown in Fig. 18 and Fig. 24, the efficiency of proposed motor is generally lower than that of benchmark IPMSM about 3~4 % of efficiency on the average. Particularly, lower efficiency of the low-speed range is remarkable.

C. Loss Details and torque ripple

Figure 25 and Fig. 26 shows the measured loss details of benchmark IPMSM and proposed motor under low-load, and middle-load operation point. The iron loss caused by PM of benchmark IPMSM is derived by subtracting the iron loss and other losses of reluctance motor (with non-magnetized PM) from the iron loss and other losses of IPMSM (with magnetized PM). The diode loss is derived by the product between the diode resistance and the averaged field current. As shown in Fig. 25, the iron loss caused by PM magnetic flux is extremely large under low-load driving point, however, the copper loss increases under middle-load area. On the other hand, iron loss of proposed motor is large compared with benchmark IPMSM as shown in Fig. 26. The space harmonic reduction, which is not utilized for self-excitation, is important to improve the efficiency of proposed motor.

Figure 27 shows the driving performance under no-load. As shown in this figure, the superior point of proposed motor can be confirmed, that is low no-load loss and no cogging torque. This is because no space harmonic occurs under no-load.

Figure 28 shows the measured torque ripple for 100 r/min. The experimental condition is limited in the extremely low-speed because of the limitation of sampling rates of torque sensor. The large torque ripple in the extremely low speed is disadvantages of proposed motor compared with benchmark IPMSM. Under this driving condition, enough rotor magnetization power cannot obtain, so that the large permeance variation increase the torque ripple.

VI. CONCLUSION

This paper has presented a PM-free synchronous motor where space harmonic power is utilized for field magnetization instead of permanent magnets. The effect of the auxiliary poles placed on the *q*-axis has experimentally discussed. In addition, verification of the self-excitation principle generated by the space harmonics power has been demonstrated, and the efficiency map is revealed through the experimental test results. Furthermore, it was investigated about the performance difference between the conventional IPMSM with Nd-Fe-B magnet and the proposed PM-free motor, experimentally. On the other hand, the proposed motor has disadvantages due to the low torque density in the

extremely low speed range. The effective solution for this problem is flux-intensifying control with time harmonic injection using pulse current command during effective periods. It will be experimentally verified as a future work. Furthermore, it is also important to develop the more accurate mathematical model since estimation of the induced current and the field current of the rotor windings is significantly important for the proposed motor to measure rotor winding heating strategy without any sensor.

REFERENCES

[1] Momoh. O. D., and Omoigui. M. O, "An Overview of Hybrid Electric Vehicle Technology," *IEEE Vehicle Power and Propulsion Conference 2009 (VPPC '09)*, pp. 1286-1292, Sept. 2009.

[2] Frieske. B., Kloetzke. M., and Mauser. F., "Trends in Vehicle Concept and Key Technology Development for Hybrid and Battery Electric Vehicles," *IEEE Electric Vehicle Symposium and Exhibition (EVS 27), 2013 World,* pp. 1-12, Nov. 2013.

[3] T. Nakada, S. Ishikawa, and S. Oki, "Development of an Electric Motor for a Newly Developed Electric Vehicle," *SAE Technical Paper,* 2014-01-1879, Apr. 2014.

[4] A. Kimura, I. Ando, and K. Itagaki, "Development of Hybrid System for SUV," *SAE Technical Paper,* 2005-01-0273, Apr. 2014.

[5] M. Natsumeda, "Motor Design Method Using Dy Diffused Magnets and Effect of its Application," *Hitachi Metals Technical Review*, Vol. 28, pp. 8-13, 2012.

[6] Stancu. C., Ward. T., Rahman. K., Dawsey. R., and Savagian. P., "Separately Excited Synchronous Motor with Rotary Transformer for Hybrid Vehicle Application," *IEEE Energy Conversion Congress and Exposition (ECCE2014),* pp. 5844-5851, Sept. 2014.

[7] C. Pollock, H. Pollock, R. Barron, J. R. Coles, D. Moule, A. Court, and R. Sutton, "Flux Switching Motors for Automotive Applications," *IEEE Trans. I. A.,* Vol. 42, No. 5, pp. 1177-1184, 2006.

[8] T. Kosaka, N. Matsui, Y. Kamada, and H. Kajiura, "Experimental Drive Performance Evaluation of High Power Density Wound Field Flux Switching Motor for Automotive Applications," *The 7th IET International Conference on Power Electronics, Machines and Drives (PEMD),* B8. 01-0418, 2014.

[9] K. Hiramoto, H. Nakai, E. Yamada, N. Minoshima, and M. Seguchi, "Rotary Electric Machine and Driving Controller for Rotary Electric Machine," US20100259136 (Published in 2010).

[10] K. Hiramoto, H. Nakai, Y. Kano, E. Yamada, and R. Mizutani, "Proposal and Feasibility Study of the Integrated Diode Synchronous Motor," *IEEJ Trans. I.A.,* Vol. 136, No. 1, pp. 54-60, 2016. (in Japanese)

[11] K. Hiramoto, H. Nakai, E. Yamada, and R. Mizutani, "An Application of the Integrated Diode Synchronous Motor to Traction Drive Motors," *IEEJ Industry Applications Society Conference.,* Vol. III, No. 3-26, pp. 187-192, 2014. (in Japanese)

[12] S. Nonaka, "The Self-Excited Type Single-Phase Synchronous Motor," *IEEJ Trans.,* Vol. 78, No. 842, pp. 1430-1438, Nov. 1958. (in Japanese)

[13] T. Fukami, Y. Hanada, and T. Miyamoto, "Analysis of the Self-Excited Three-Phase Synchronous Generator Utilizing the 2nd-Space Harmonic for Excitation," *IEEJ Trans. I.A.,* Vol. 117, No. 1, pp. 57-65, 1997. (in Japanese)

[14] L. F. A. Izzat, and S. Heier, "Development in Design of Brushless Self-Excited and Self-Regulated Synchronous Generator," *IEEE The 2nd International Conference on Renewable Energy Research and Applications (ICRERA),* ID:374, pp. 1024-1029, Oct. 2013.

[15] J. Oyama, S. Toba, T. Higuchi, and E. Yamada, "The Principle and Fundamental Characteristics of Half-Wave Rectified Brushless Synchronous Motor," *IEEJ Trans. I.A.,* Vol. 107, No. 10, pp. 1257-1264, 1987. (in Japanese)

[16] S. Nonaka, and T. Kawaguchi, "A New Variable-Speed AC Generator System Using a Brushless Self-Excited-Type Synchronous Machine," *IEEE Trans. I.A.,* Vol. 1, pp. 691-696, Oct. 1990.

[17] M. Aoyama, and T. Noguchi, "Preliminary Study on Rare-Earth Free Motor with Field Pole Excited by Space Harmonics," *IEEJ Annual Meeting,* No. 5-051, pp. 91-92, Mar. 2013. (in Japanese)

[18] M. Aoyama, and T. Noguchi, "Torque Performance Improvement with Modified Rotor Winding Circuit of Wound-Field Synchronous Motor Self-Excited by Space Harmonics," *IEEJ Trans. I.A.,* Vol. 134, No. 12, pp. 1038-1049, Dec. 2014. (in Japanese)

[19] M. Aoyama, and T. Noguchi, "Experimental Verification of Radial-Air-Gap-Type Permanent-Magnet-Free Synchronous Motor Utilizing Space Harmonics with Auxiliary Poles," *IEEJ Trans. I.A.,* Vol. 135, No. 8, pp. 869-881, Aug. 2015. (in Japanese)

[20] M. Aoyama, and T. Noguchi, "Preliminary Experimental Verification of Self-Excited Wound-Field Synchronous Motor with Auxiliary Poles for Automotive Applications," *IEEE International Conference on Industrial Technology* (*ICIT*)*,* pp. 818-824, 2015.

[21] M. Aoyama, "The IPM Motor Distributed Magnetic-path and had a *d*-axis Cavity for Optimization of the amount of Magnet," *IEEJ Technical Meeting,* VT-13-015, pp. 1-5, Mar. 2013. (in Japanese)